RSC Advances

PAPER

View Article Online
View Journal | View Issue

Cite this: *RSC Adv.*, 2014, **4**, 48734

Fostering the properties of $Zr_{0.8}Sn_{0.2}TiO_4$ (ZST) ceramics *via* freeze granulation without sintering additives

S. M. Olhero,* Ajay Kaushal* and J. M. F. Ferreira

Received 4th June 2014
Accepted 16th September 2014

DOI: 10.1039/c4ra05323k

www.rsc.org/advances

The present paper reports the overall benefits of freeze granulation for enhancing the properties of zirconium tin titanate $Zr_{0.8}Sn_{0.2}TiO_4$ (ZST) ceramics in the total absence of sintering additives. The ZST powder was synthesized by solid state reaction and attrition milled in ethanol for 10 h. This starting non-granulated powder (NG-ZST), without and with 1 wt% ZnO as sintering additive, was used to consolidate green bodies by dry pressing. The pure ZST powder was also dispersed in aqueous media to obtain stable suspensions with high solid loadings. Free flowing spherical homogeneous granules were prepared by freeze granulation and used to consolidate ZST green bodies by dry pressing (FG-ZST). The effects of processing variables and sintering temperature (1300 1450 °C) on densification and on the structural, mechanical and electrical properties of ZST ceramics were systematically investigated. Our study clearly reveals the superior properties of FG-ZST ceramics, which derive from an enhanced sintering behaviour associated with the absence of sintering additives.

A Introduction

The synthesis and structural characterization of zirconium titanate ($ZrTiO_4$) based materials for applications as resonator components in microwave devices have recently attracted considerable and growing interest.[1] $ZrTiO_4$ ceramic material exhibits the α-PbO orthorhombic structure that transforms into the rutile structure of $TiO_2(SnO_2)$ at a certain Sn content. When Zr ions are substituted with Sn ions, a temperature stable $(Zr,Sn)TiO_4$ microwave resonator is obtained by interfering with the ordering of metal ions that results in improved dielectric properties. There is a phase boundary at $x = 0.3$ in $Zr_{1-x}Sn_xTiO_4$; at $x < 0.3$, a single-phase $(Zr,Sn)TiO_4$ exists; but for $x > 0.3$, secondary phases of rutile $(Ti,Sn)O_2$ coexist with $(Zr,Sn)TiO_4$.[2,3] Therefore, the solid solutions of zirconium tin titanate ($Zr_{1-x}Sn_xTiO_4$; $0 < x \leq 0.2$) have been considered to be potential materials for use in dielectric resonators or filters operating at microwave frequency because of their high quality factor ($Q > 3000$), high dielectric constant ($\varepsilon_r > 25$), and low temperature coefficient of resonant frequency (TCF < ±10 ppm °C^{-1}).[4 10] The ZST ceramics are traditionally consolidated from spray-dried powders. Unfortunately, this granulation method is prone to the formation of cavities, strong interparticle bonds and the migration of additives and/or smaller particles to the granule surface. Such heterogeneities exacerbate the difficulties for completely densifying $Zr_{1-x}Sn_xTiO_4$ ceramics without the aid of sintering additives. Some common sintering aids used for $Zr_{1-x}Sn_xTiO_4$ ceramics are added as a combination of two or more oxides from the group consisting of ZnO, CuO, La_2O_3, NiO, Fe_2O_3, B_2O_3, Bi_2O_3, and V_2O_5.[11 14] However, sintering aids affect the ceramics in many ways by changing density, microstructure, defect structure, and possibly crystal structure. These changes, caused by the sintering aids, affect the resulting dielectric properties. Many earlier investigations on $Zr_{1-x}Sn_xTiO_4$ compositions and other microwave dielectrics showed that the selection of proper additives and their optimum quantity is effective in enhancing the dielectric properties. A higher relative density results in a higher dielectric constant.[15,16] Therefore, improving the sintering ability and various functional properties of zirconium tin titanate ceramics without using sintering aids has been a challenging task. Accomplishing this task demands an upgrade in the powder processing approach to improve particle packing ability and achieve high density and homogeneous green compacts upon consolidation. Such potential gains derived from processing could be a way to exclude sintering additives from $Zr_{1-x}Sn_xTiO_4$ compositions. Our recent findings[15,17,18] stimulated us to achieve the successful aqueous colloidal processing of $Zr_{1-x}Sn_xTiO_4$ composition and further prepare high quality spherical granules by freeze granulation (FG), resulting in ceramics with high green dense compact on consolidation. FG can help ceramic manufacturers achieve powder formulations with superior homogeneity, pressing performance and dispersibility.[19 21] During FG, droplets are rapidly frozen in liquid nitrogen before being recovered and subsequently freeze-dried. Freezing being a fast process, diffusion dynamics are insufficient to induce any binder

Department of Materials and Ceramic Engineering, CICECO, University of Aveiro, 3810 193, Aveiro, Portugal. E mail: susana.olhero@ua.pt; ajay.kaushal@ua.pt; Fax: +351 234 370204; Tel: +351 234 370354

migration, thereby better preserving the granule homogeneity.[22,23] Contrary to spray drying, the freeze dried granules do not shrink during freeze drying, maintaining their spherical shapes and consequently allowing high granule deformability. Recognizing the advantages of FG, Stuer *et al.*[20] adopted FG powders as an industrially viable alternative to loose powder for sintering transparent polycrystalline alumina. Hence, the FG method provides granules with a high degree of homogeneity that can be easily broken down in a subsequent processing step such as pressing or re-dispersing in a liquid. The composition of $Zr_{0.8}Sn_{0.2}TiO_4$ (ZST) was chosen for the present investigation because it is phase pure and stable against thermal decomposition.[24] The ZST powder with this composition was successfully dispersed in water and the suspension was sprayed against liquid nitrogen to obtain homogeneous granules. The benefits of FG for the consolidation/sintering steps were highlighted by comparing the green and sintered density values of ZST ceramics prepared by dry pressing from FG powder and non-granulated powders (NG) without and with 1 wt% ZnO as sintering additive. The effects of sintering temperature (T_{sint}) that was varied within the range from 1300 to 1450 °C on the various structural, mechanical and dielectric properties of the as-obtained ZST ceramics were investigated. The search was for processing conditions that could lead to low-loss dielectric ZST materials within the microwave frequency range.

B Experimental

B.1 Powder synthesis

The zirconium tin titanate powder (ZST) ($Zr_{0.8}Sn_{0.2}TiO_4$) was synthesized through the conventional solid state reaction process from high purity ZrO_2 (zirconium oxide, Sigma-Aldrich, Steinheim, Germany), SnO_2 (tin IV oxide, Sigma-Aldrich, Steinheim, Germany) and TiO_2 (titanium IV oxide, Riedel-de Haën, Seelze, Germany). The starting raw materials were mixed according to the required stoichiometric proportions and dry ball-milled for 2 h to guarantee complete homogenisation. The precursor mixture was first calcined at 1100 °C for 2 h, dry ball-milled for 2 h, and then subjected to a second heat treatment for 2 h at 1350 °C. To reduce the particle size of the calcined powder, attrition milling at 700 rpm speed in ethanol was conducted for 10 h. The efficacy of the deagglomeration progress was monitored by particle size analysis using a light scattering technique (Beckman Coulter LS 230, CA USA; Fraunhofer optical model). For this, approximately 0.1 g of dry-milled powder was dispersed into 50 ml of distilled water followed by 20 minute of ultrasonic treatment to separate the powdered particles. The resultant diluted suspension was analyzed for particle size distribution. Three measurements per sample were performed to confirm the reproducibility of the distribution curves. The resultant ZST slurry was dried at 110 °C and characterised by X-ray diffraction (Rigaku, Tokyo, Japan), specific surface area (BET, Gemini, Micromeritics, USA) and helium pycnometry (Multipycnometer, Quantachrome Instruments, USA), and used for further studies in the pure non-granulated (NG-ZST) and freeze granulated (FG-ZST) forms with the addition of 1 wt% ZnO as sintering additive, as detailed below.

B.2 Investigating the effects of freeze granulation and ZnO-doping

Successful freeze granulation requires a suitable balance between low viscosity and high concentrated suspensions. Therefore, the dispersion ability of the ZST powder in aqueous media was first investigated to establish the optimal processing conditions. The potential at the solid/liquid interface was assessed by Zeta-potential measurements (Delsa 440 Sx, Coulter, Buckinghamshire, UK) in the absence and presence of dispersant (Dispex A40). The powders were suspended in a 1 mM KCl solution as background electrolyte to ensure a constant ionic strength. Each suspension was divided in two equal parts for increasing and decreasing pH runs, and the pH values were adjusted by using 0.1 M solutions of either KOH or HCl. The efficacy of Dispex A40 in dispersing the ZST powder was further confirmed by the ease with which the aqueous slurries containing 40, 45 and 50 vol% could be prepared by adding 0.5 wt% dispersant. The suspensions were deagglomerated for 24 h in polypropylene bottles using zirconia balls (the charge-to-balls ratio was 1 : 3). The viscosity of slurries was measured using a rotational Rheometer (Bohlin C-VOR Instruments, Worcestershire, UK) equipped with a cone and plate (4°, 40 mm, and gap of 150 μm) measuring configuration. The flow measurements were conducted between 0.1 and 500 s^{-1}. A binder emulsion (Duramax B1000, Rohm and Haas, Lauterbourg, France) was added (3 wt% relative to the dry powder) to the ZST suspension containing 45 vol%. This aqueous suspension was sprayed into liquid nitrogen (196 °C) to obtain granules by freeze granulation (PowderPro freeze granulator LS-2, Gothenburg, Sweden). The LS-2 freeze granulator consists of a slip container with a stirrer, a pump for the slip, a spray nozzle, a regulator for compressed air and an insulated chamber for liquid nitrogen to spray and collect freeze granules. Prior to the granulation process, the ZST suspension was filtered using a 120 μm sieve to safely avoid any agglomeration that may obstruct flow through the 1.20 mm diameter granulation nozzle. For successful micro sized ZST granulation, the suspension was sprayed at a pumping speed of 30 rpm with ~0.8 bar air pressure. A drying step at 49 °C under a pressure of 0.133 Pa (1×10^{-3} Torr) in a freeze-drying system (Labconco, LYPH Lock 4.5, Kansas City, MO) was then conducted for 72 h. The freeze dried (FG-ZST) granules were uniaxially pressed into disc-shaped pellets (20 mm diameter, 3–5 mm thickness) and bars (50 mm × 5 mm × 5 mm) at a uniaxial pressure of 60 MPa, followed by isostatic pressing at 200 MPa.

Dry pressing was similarly adopted to consolidate green bodies from the starting powder, either pure (NG-ZST) or doped, with ZnO as sintering additive. In the last case, the starting NG-ZST powder was mixed in ethanol with 1 wt% ZnO (NG-ZST–ZnO) followed by drying. The same type and amount of binder (Duramax B1000, 3 wt% relative to the dry mass) was added to the dried NG-ZST and NG-ZST–ZnO powders by spraying and mixing in a mortar. Binder burnout of all the samples was performed at a heating rate of 1 °C min^{-1} up to 600 °C with a holding time of 1 h at this temperature. Sintering was performed at different temperatures (1300, 1350, 1400 and 1450 °C)

at a heating rate of 5 °C min^{-1}, holding for 4 h at the set temperature, followed by natural cooling. Dilatometry measurements were performed on bar shaped (50 mm × 5 mm × 5 mm) green samples of NG-ZST, FG-ZST, and NG-ZST FG using a Dil 801L dilatometer (BAHR Thermoanalyse, GmbH, Germany). The complete dilatometric shrinkage data were measured from room temperature (RT) to 1400 °C at a heating rate of 10 °C $minute^{-1}$ in air atmosphere.

B.3 Characterization of ZST sintered samples

The crystallinity of the ZST synthesised powder and the sintered samples at different temperatures (1300–1450 °C) were studied using a Rigaku X-ray diffractometer of CuK_α (1.54 Å) radiations in θ–2θ geometry. Bulk density (ρ_{bulk}) of sintered ZST ceramics was measured in ethylene glycol according to the Archimedes principle (ASTM C372, ASTM International, West Conshohocken, PA) using a Mettler balance (AG 245, Mettler Toledo, Zurich, Switzerland). Three density measurements were performed for each kind of ceramic sample and the results are expressed as the average. Maximum experimental error was systematically $<\pm 0.01$. Surface fracture microstructures of sintered ceramics were obtained by scanning electron microscopy (SEM, JSM-5410, JEOL, Tokyo, Japan) with an energy-dispersive scanning attachment (Sigma 3.42 Quaser, Kevex Instruments, Stanford, Valencia, CA).

Vickers microhardness measurements were performed on sintered and polished ZST samples using Struers Duramin testing equipment (Struers, Denmark). Three-point bending tests were conducted in a Shimadzu Autograph AG-X-1kN Universal Testing Machine (Kyoto, Japan). The cavity method was used for measuring dielectric constant and quality factor. In this method, we measure the shift in the resonant frequency of the cavity, Δf, caused by the sample and related to the real part of the complex permittivity, ε', while the change in the inverse of the quality factor of the cavity, $\Delta(1/Q)$, gives the imaginary part, ε''. The measurements were made using an HP 8753D and a HP8361 Network Analyzer coupled to 1.0 GHz and 6.0 GHz cavity resonators.

C Results and discussion

C.1 ZST powders and suspensions

Fig. 1 shows the particle size distribution (PSD) of sintered ZST powders before (dry ball milled for 1 h) and after wet attrition milling (AM) for 10 h in ethanol. The powder that was dry milled for 1 h has an average particle size of ~9 μm and exhibits a trimodal distribution with fine and coarse populations centred at ~0.2 μm and ~27 μm, respectively, and a main intermediate population centred at ~6 μm. Both the intermediate and (especially) coarser populations reveal the presence of particle agglomerates. Attrition milling completely destroyed the third population of agglomerates, reduced drastically the second one and shifted the remaining part to smaller sizes, while significantly increasing the population of fine particles. The resulting AM powder with an average particle size of ~0.4 μm exhibits a bimodal size distribution adequate to prepare highly concentrated colloidal suspensions. A bimodal PSD enhances the packing ability of the system and decreases the viscosity of a suspension at a given solid loading, facilitating the flow through a fine nozzle during freeze granulation. The resultant ZST powder after 10 h AM presented a BET specific surface area of 3.2 $m^2\ g^{-1}$ and a theoretical density of 5.19 g cm^{-3}.

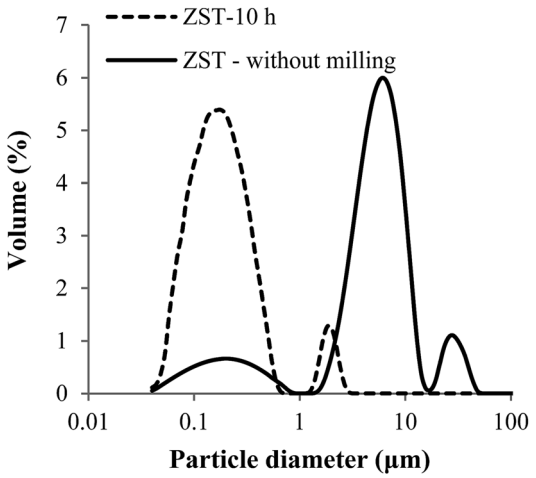

Fig. 1 Particle size distribution of the as-synthesized ZST powder (without milling) and after 10 h of attrition milling.

To assess the effects of dispersant (Dispex A-40) on the electrostatic repulsion between the ZST particles, Zeta potential measurements were performed in the absence and the presence of dispersant. The curves displayed in Fig. 2 reveal an isoelectric point (IEP) at pH ≈ 3 for the naked ZST particles and a dislocation of the entire electrophoretic curve towards more negative Zeta potential values lower slightly towards the acidic region. This resulted in a shift of the IEP to pH ≈ 2. It is well-known that for low values of Zeta potential, intermolecular attractive forces between particles tend to exceed the electrostatic repulsive ones, resulting in a flocculated system. An opposite scenario is required for colloidal particles to form stable suspensions. The Zeta potential values measured at the natural pH of the suspensions in the presence of dispersant (pH ≈ 9) are high enough (80 mV) to keep high repulsion between particles, and consequently for allowing the preparation of

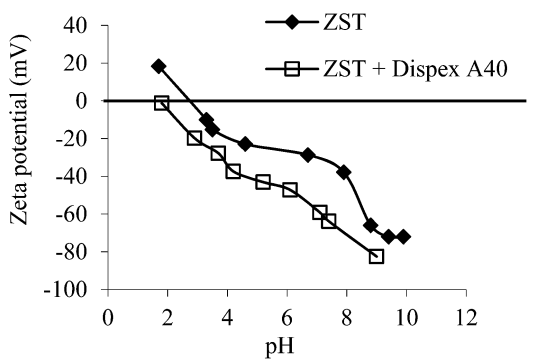

Fig. 2 Zeta potential of the ZST powder in the absence and the presence of dispersant.

highly concentrated suspensions of ZST powders in aqueous media. This is confirmed by the rheological measurements performed on ZST suspensions with different solid loadings (Φ = 40, 45 and 50 vol%) within the range from $\dot{\gamma}$ = 0.1–500 s^{-1}. The viscosity (η_s) *vs.* shear rate ($\dot{\gamma}$) dependence curves presented in Fig. 3 show that all the suspensions displayed shear thinning behaviour within the entire $\dot{\gamma}$ range, which is a characteristic of well-dispersed and highly concentrated systems. The shear thinning flow behaviour reveals that particle aggregates in the suspensions are gradually broken down into smaller flow units by the applied forces such that the resistance to flow is reduced, leading to lower viscosity with increasing shear rate. The particles become less and less interactive as the solid volume fraction decreases. The ZST suspension with 45 vol% solid loading was selected to prepare granules by FG. Fig. 4 shows the SEM images of green ZST granules obtained by freeze-drying. Spherical granules with diameters within the range of a few hundreds of micrometres were obtained. These morphological/size features confer them free flow behaviour and low friction with die walls upon dry pressing, which are essential features for obtaining homogeneous and highly dense ZST compacts.

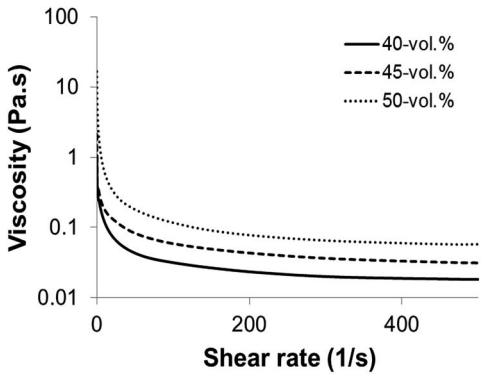

Fig. 3 Flow curves of the ZST suspensions in aqueous media containing different solid loadings (40, 45 and 50 vol%).

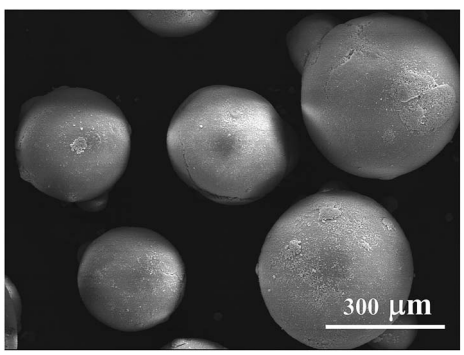

Fig. 4 ZST granules (green state) obtained by freeze granulation from an aqueous suspension containing 45 vol% solids.

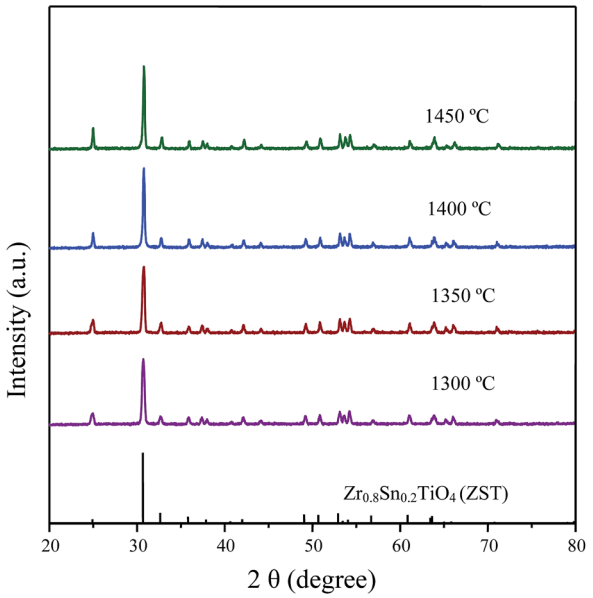

Fig. 5 XRD patterns of pure $Zr_{0.8}Sn_{0.2}TiO_4$ (ZST) ceramics sintered at different temperatures (1300, 1350, 1400, 1450 °C).

C.2 Structural properties of sintered ZST ceramics

Fig. 5 shows the XRD patterns of the pure ZST ceramics sintered at different T_{sint} of 1300, 1350, 1400 and 1450 °C. All the diffraction peaks of the ZST ceramics correspond to orthorhombic-type phase structure in agreement with the respective Joint Committee on Powder Diffraction Standards (JCPDS) card no. 01-081-2214, and are consistent with the results reported elsewhere.[25] The intensity of the dominant peak (observed at ~31°) was found to increase with increasing T_{sint}. This apparent enhancement in the crystallinity of the ZST phase is probably due to favourable crystal growth kinetics with increasing temperature.

Table 1 reports the physical/mechanical properties [relative density (ρ_r), microhardness and flexural resistance] of the investigated ZST ceramics sintered at different temperatures. Irrespective of the specific processing parameters used, a general increasing trend of ρ_r with increasing T_{sint} is observed. Interestingly, significantly higher ρ_r values were measured for the samples consolidated from the freeze granulated (FG-ZST) powder in comparison to those derived from the non-granulated (NG-ZST) one. In the last case, ρ_r changed from 84% (1300 °C) to 93% (1450 °C) (based on the theoretical density of ZST = 5.19 g cm^{-3}). This value is even 2.4% lower than that achieved for FG-ZST compacts upon sintering at the lowest sintering temperature tested (1300 °C). The observed differences suggest that the diffusion paths have been shortened in the samples derived from the FG powder due to their higher degree of homogeneity. In general, micron-sized granules obtained by freeze granulation exhibit a number of favourable features in comparison to loose powders or granules obtained by spray drying as follows: (i) have lower green density in comparison to granules obtained by spray drying; (ii) are homogeneous (no binder segregation occurs); (iii) have free-flowing behaviour that enables their spatial rearrangements; and (iv) are easily smashed under the applied pressure. These features favour the elimination of intergranular pores. The

Table 1 Relative density, microhardness and flexural resistance of ZST samples consolidated by dry pressing from ZST powders non-granulated (NG-ZST), freeze granulated (FG-ZST) and non-granulated with added 1 wt% ZnO as sintering additive (NG-ZST ZnO)

Samples	T_{sint} (°C)	Relative density, ρ_r (%TD)	Microhardness (MPa)	Flexural resistance (MPa)
NG ZST	1300	84.0 ± 1.6		54.0 ± 11.7
	1350	87.6 ± 7.6	1226.3 ± 165.6	74.3 ± 14.1
	1400	89.4 ± 3.2	4030.5 ± 719.4	87.6 ± 20.8
	1450	93.0 ± 0.7	6610.2 ± 500.2	119.2 ± 43.3
FG ZST	1300	96.4 ± 2.4	3602.2 ± 249.7	104.0 ± 16.3
	1350	96.9 ± 1.2	6248.4 ± 481.2	141.3 ± 8.1
	1400	98.7 ± 0.7	9527.0 ± 441.3	179.7 ± 45.8
	1450	97.2 ± 0.4	9135.1 ± 433.3	157.2 ± 17.4
NG ZST ZnO	1300	96.9 ± 0.5	4189.7 ± 549.2	121.2 ± 36.6
	1350	97.4 ± 1.8	6893.2 ± 379.8	154.4 ± 27.0
	1400	98.9 ± 0.9	9679.1 ± 563.1	181.8 ± 13.7
	1450	97.5 ± 0.7	9372.3 ± 491.5	167.5 ± 23.9

binder in FG granules acts as a lubricant, assisting primary particles sliding and rearranging to increase packing efficiency and compact density. An increase in packing efficiency and compact density will enhance the densification ability upon sintering while implying a decrease in total shrinkage.[15,18] This is confirmed by the data plotted in Fig. 6 that compares the dilatometry curves of all types of powder compacts (FG-ZST, NG-ZST and NG-ZST–ZnO) monitored within the temperature range from room temperature (RT) to 1400 °C. The FG-ZST curve exhibits a negative inclination along the lower temperature range probably because of the homogeneous distribution of binder among the particles, and its burnout enables the particles to gradually approach each other. The positive inclination observed for NG-ZST and NG-ZST–ZnO curves reveals that thermal expansion along this lower temperature range predominates over any shrinkage. Fig. 6 reveals that the onset of shrinkage due to sintering occurs earlier (~950 °C) and progresses at a much faster rate for the NG-ZST–ZnO sample, which achieved a minimum in the curve at ~1260 °C followed by a slope reversion due to the predominance of dilatation over shrinkage. This effect justifies the use of ZnO as the sintering additive.[12,13] The onset of shrinkage due to sintering for the NG-ZST occured roughly at ~1050 °C, and its densification process was still far from completion at the maximum tested temperature of 1400 °C. In contrast, a downshift of ~50 °C in the onset of shrinkage and much faster densification kinetics are observed in the case of FG-ZST. These features clearly indicate the benefits of freeze granulation as a viable route for obtaining high density pure ZST ceramics and avoiding external doping that might compromise their functional properties. The ρ_r values of FG-ZST and NG-ZST–ZnO ceramics sintered at 1400 °C are close to ~99%, and their mechanical properties (microhardness and flexural resistance) are also comparable (Table 1). Slightly decreasing trends are observed for ρ_r and mechanical properties of the FG-ZST and NG-ZST–ZnO samples with further increasing T_{sint} to 1450 °C. These are attributed to an over firing effect as suggested by the increasing size of intergranular pore, as seen in the SEM micrographs of fracture surfaces shown in Fig. 7. Fig. 7a–f shows the SEM images of polished surfaces of NG-ZST, FG-ZST and NG-ZST–ZnO ceramics sintered at high T_{sint} of 1400 and 1450 °C, revealing different microstructural features. The selection of these two high T_{sint} to investigate the microstructural features was based on the dilatometric curves, which suggested that maximum densification was achieved for FG-ZST and NG-ZST–ZnO, contrasting with the NG-ZST ceramics. These SEM images reveal different morphological features that reflect different sintering ability between FG-ZST and NG-ZST ceramics, which derive solely from the powders undergoing freeze granulation and how this processing step affects consolidation. In the case of NG-ZST ceramics, the porosity fraction was found to decrease with increase in T_{sint} from 1400 °C to 1450 °C (Fig. 7a and b), in good agreement with density data reported in Table 1 that showed a steady increase from 84 to 93% with sintering temperature increasing from 1300–1450 °C. This contrasts with the observations made for FG-ZST and NG-ZST–ZnO ceramics sintered at 1400 °C and 1450 °C (Fig. 7c–f) that show larger pores derived from pore coalescence. These structural changes suggest that an over firing

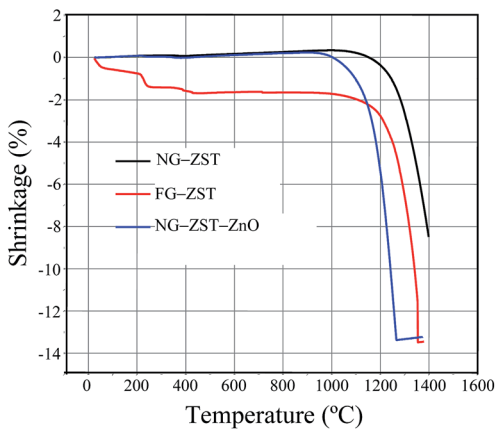

Fig. 6 Dilatometry analysis of green bodies consolidated from powders NG-ZST, FG-ZST, and NG-ZST with added 1 wt% ZnO as sintering additive (NG-ZST ZnO) performed within the temperature range from RT to 1400 °C.

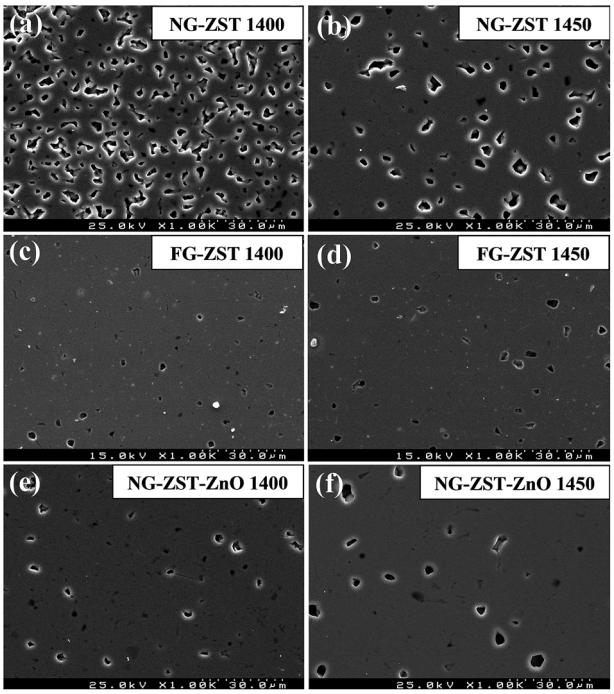

Fig. 7 SEM images of polished surfaces of ZST ceramics derived from NG-ZST, FG-ZST and NG-ZST ZnO powders revealing the effects of processing variables and sintering temperature (1400 and 1450 °C) on microstructural features.

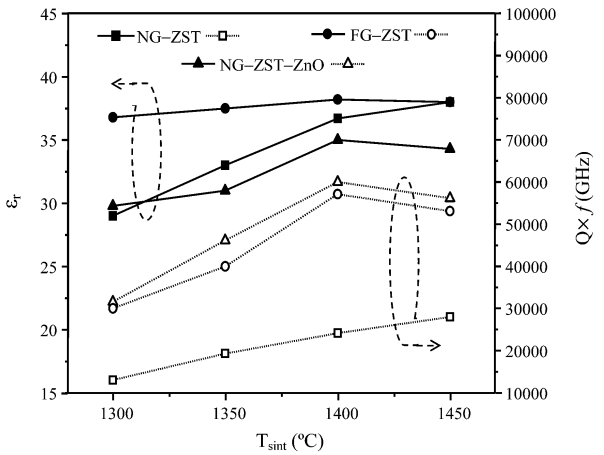

Fig. 8 Dielectric constant (ε_r) (solid symbol and lines) and $Q \times f$ (open symbol and lines) measured at 6 GHz (microwave frequency) for ZST ceramics derived from NG-ZST, FG-ZST and NG-ZST ZnO powders and sintered at different temperatures (1300, 1350, 1400 and 1450 °C).

effect occurred in the FG and ZnO added ZST ceramics sintered at 1450 °C, which is in good agreement with density data reported in Table 1. These results confirm that all the thermal events occur at lower temperatures for ceramics consolidated from FG powder due to its enhanced homogeneity in comparison to ceramics derived from NG powders.

The larger crystallite size FG-ZST ceramics in comparison to that of NG-ZST can be easily explained in terms of diffusion kinetics. The compacts derived from uniform FG-ZST powders enable obtaining a homogeneous distribution of fine pores and higher green densities in comparison to NG-ZST ones. These conditions constitute the main driving force for diffusion processes upon sintering that lead to faster densification and grain growth in the case of FG-ZST samples. Upon sintering, most of the very small pores tend to disappear and the sintered density achieves a maximum value at a given temperature. Beyond this temperature, density is likely to decrease due to pore coalescence, or the eventual formation of gases due to the volatilisation of some components, known as over firing effect. This appears to occur in the FG-ZST and ZnO added ZST ceramics sintered at 1450 °C.

C.3 Microwave dielectric properties (Q factor) of ZST ceramics

Fig. 8 shows the room temperature dielectric constant (ε_r) and quality factor (Q) values measured at 6 GHz (microwave frequency) for the NG-ZST, FG-ZST and NG-ZST–ZnO ceramics sintered at different T_{sint} of 1300, 1350, 1400 and 1450 °C. The gathered data are also reported in Table 2. The ε_r values of all the prepared ZST ceramics were found to vary in the range from 25 to 38.2 with the highest one being observed for FG-ZST sintered at 1400 °C. The NG-ZST–ZnO ceramics exhibit a maximum $\varepsilon_r = 35$ when sintered at 1400 °C, being even lower than that measured for NG-ZST ceramics. Except for the NG-ZST ceramics sintered at the lowest temperature, it can be observed that pure ZST ceramics exhibit higher ε_r values in comparison to the NG-ZST–ZnO ones. This confirms the deleterious effect of the dielectric constant for doping the ZST with 1 wt% ZnO. On the other hand, the loss, quality factor (Q) values are the highest for the NG-ZST–ZnO ceramics at the entire T_{sint} range in comparison to pure ZST ceramics. This can be attributed to larger grain sizes observed in the SEM micrographs of Fig. 7 with fewer grain boundaries contributing to the loss. However, the Q values measured for FG-ZST are relatively close to those of NG-ZST–ZnO ceramics at any T_{sint} tested. The Q values for pure ZST

Table 2 Dielectric constant and $Q \times f$ factor of the ZST ceramics sintered at different temperatures and consolidated by dry pressing from ZST powders non-granulated (NG-ZST), freeze granulated (FG-ZST) and non-granulated with added 1 wt% ZnO as sintering additive (NG-ZST ZnO)

	Dielectric constant (ε_r) (at 6 GHz)			$Q \times f$ (at 6 GHz) (GHz)		
T_{sint} (°C)	NG ZST	FG ZST	NG ZST ZnO	NG ZST	FG ZST	NG ZST ZnO
1300	29.0	36.8	29.8	13 043	30 000	31 579
1350	33.0	37.5	31.0	19 286	40 000	46 156
1400	36.7	38.2	35.0	24 182	57 143	60 000
1450	38.0	38.0	34.3	28 000	53 078	56 154

ceramics were found to improve with increasing ρ_r and grain size and are significantly higher for the samples consolidated from FG powder and shown in Fig. 8. The maximum $Q \times f$ value of FG-ZST ceramics sintered at 1400 °C (57 143 GHz) is considerably higher than the maximum of 28 000 GHz measured for NG-ZST ceramics sintered at 1450 °C. The comparison of Fig. 8 with data reported in Tables 1 and 2 enables concluding that ε_r and $Q \times f$ values scale well with ρ_r and show good consistency with microstructural features.

Conclusions

Micron-sized granules of ZST powder *via* a freeze granulation method were successfully fabricated *via* spraying a stable aqueous suspension into liquid nitrogen (freeze granulation), followed by freeze drying. It was demonstrated that FG results in a number of benefits, including a higher degree of homogeneity in the binder distribution, an enhanced packing ability of the powders, and a faster sintering kinetics. These features enable the improvement of the final physical/mechanical and dielectric properties of the ceramics and achieving the maximum at lower sintering temperatures. Another advantage of the FG approach is the possibility to avoid the addition of sintering additives that might degrade the required functional properties. A maximum $Q \times f$ value of 57 143 GHz was measured for the FG-ZST ceramics sintered at 1400 °C, which is about double of that found for NG-ZST ceramics (28 000 GHz) when sintered at a higher temperature of 1450 °C. All the relevant physical and electrical properties of ZST ceramics revealed good correlations with sintered density, which in turn was shown to be strongly dependent on the quality of processing translated by the homogeneity of green compacts.

Acknowledgements

S.M. Olhero and Ajay Kaushal are thankful to the Foundation for Science and Technology of Portugal (FCT) for financial support under the grant SFRH/BPD/87486/2012 and SFRH/BPD/77598/2011, respectively, and the financial support under the project PTDC/CTM/099489/2008. The support from CICECO is also acknowledged.

Notes and references

1 A. Borrell, M. D. Salvador, V. G. Rocha, A. Fernández, A. Gómez, E. López-López and R. Moreno, *Composites, Part B*, 2014, **56**, 330.
2 W. Wersing, High Frequency ceramic dielectric and their application for microwave components, in *Electronic ceramics*, ed. B. C. H. Steele, Elsevier Science Publishers LTD, Barking, UK, 1991, ch. 4, p. 67.
3 S. Hirano, T. Hayashi and A. Hattori, *J. Am. Ceram. Soc.*, 1991, **74**, 1320.
4 C.-H. Hsu, *Thin Solid Films*, 2009, **517**, 5061.
5 C.-H. Hsu and C.-Y. Chung, *J. Alloys Compd.*, 2010, **491**, 483.
6 S. Genovesi, F. Costa, B. Cioni, V. Miceli, G. Annino, G. Gallone, G. Levita, A. Lazzeri, A. Monorchio and G. Manara, *Microw. Opt. Tech. Lett.*, 2009, **51**(11), 2753.
7 P. G. Babu, C. Kumar, K. Ravichandran and P. Manohar, *Int. J. ChemTech Res.*, 2013, **5**(5), 2122.
8 J.-M. Wu, W.-Z. Lu, W. Lei, J.-P. He and J. Wang, *Ceram. Int.*, 2011, **37**, 481.
9 K. H. Yoon and E. S. W. Kim, *Mater. Res. Bull.*, 1995, **30**(7), 813.
10 G. Huang, D. Zhou, J. Xu, X. Chen, D. Zhang, W. Lu and B. Li, *Mater. Sci. Eng., B*, 2003, **99**, 416.
11 S. Vahabzadeh, M. A. Golozar and F. Ashrafizadeh, *J. Alloys Compd.*, 2011, **509**, 1129.
12 C.-L. Huang, C.-S. Hsu and R.-J. Lin, *Mater. Res. Bull.*, 2001, **36**, 1985.
13 V. L. Abrantes, *J. Mater. Eng. Perform.*, 2012, **21**(8), 1777.
14 V. L. Abrantes and D. P. F. de Souza, *Mater. Sci. Eng., A*, 2005, **398**, 220.
15 A. Kaushal, S. M. Olhero, P. Antunes, A. Ramalho and J. M. F. Ferreira, *Mater. Res. Bull.*, 2014, **50**, 329.
16 R. Kudesia, A. E. McHale and R. L. Snyder, *J. Am. Ceram. Soc.*, 1994, **77**(12), 3215.
17 A. Kaushal, S. M. Olhero and J. M. F. Ferreira, *J. Mater. Chem. C*, 2013, **1**, 4846.
18 A. Kaushal, S. M. Olhero, B. K. Singh, V. Saravanan and J. M. F. Ferreira, *RSC Adv.*, 2014, **4**, 26993–27002.
19 B. Nyberg, E. Carlstrom and R. Carlsson, Freeze granulation of liquid phase sintered silicon carbide, in *Ceramic Transaction, Silicon-Based Structural Ceramics*, ed. B. W. Sheldon and S. C. Denforth, Americal Ceramic Society, Westerville, Ohio, 1994, vol. 42, pp. 107–113.
20 M. Stuer, Z. Zhao and P. Bowen, *J. Eur. Ceram. Soc.*, 2012, **32**, 2899.
21 J. Orlenius, O. Lyckfeldt, K. A. Kasvayee and P. Johander, *J. Power Sources*, 2012, **213**, 119.
22 O. Lyckfeldt, D. Käck and K. Rundgren, *Ceram. Eng. Sci. Proc.*, 2003, **24**(4), 331.
23 O. Lyckfeldt, K. Rundgren and M. Sjöstedt, *Key Eng. Mater.*, 2004, **264–268**(1), 281.
24 Y. H. Park, J. M. Ryu, M. Y. Shin, K. H. Ko, D. W. Kim and K.-S. Hong, *J. Am. Ceram. Soc.*, 2001, **84**, 2542.
25 R. Kudesia, R. L. Snyder, R. A. Condrate and A. E. McHale, *J. Phys. Chem. Solids*, 1993, **54**, 671.